Switchable Assembly and Guidance of Colloidal Particles on an All-Dielectric One-Dimensional Photonic Crystal

Fengya Lu, Yan Kuai, Junxue Chen, Xi Tang, Yifeng Xiang, Yang Liu, Pei Wang, Joseph. R. Lakowicz, and Douguo Zhang

Phys. Rev. Applied **13**, 014020 — Published 13 January 2020

DOI: 10.1103/PhysRevApplied.13.014020

Switchable Assembly and Guidance of Colloidal particles on an All-Dielectric One-Dimensional Photonic Crystal

Fengya Lu[1], Yan Kuai[1], Junxue Chen[2], Xi Tang[1], Yifeng Xiang[1], Yang Liu[1], Pei Wang[1], Joseph. R. Lakowicz[3], Douguo Zhang[1]*

[1] Advanced Laser Technology Laboratory of Anhui Province and Institute of Photonics, Department of Optics and Optical Engineering, University of Science and Technology of China, Hefei, Anhui, 230026, China

[2] School of Science, Southwest University of Science and Technology, Mianyang, Sichuan 621010, China.

[3]Center for Fluorescence Spectroscopy, Department of Biochemistry and Molecular Biology University of Maryland School of Medicine, 725 West Lombard St., Baltimore, MD 21201, USA.

*Correspondence and requests for materials should be addressed to D.G. Zhang. (Email: dgzhang@ustc.edu.cn)

ABSTRACT: Dielectric multilayer photonic-band-gap (PBG) structures that are called one-dimensional photonic crystals (1DPCs), have drawn considerable attentions in the field of physics, chemistry and biophotonics. Here, experimental results verify the feasibility of 1DPC working as a substrate for the switchable manipulations of colloidal microparticles. The optically induced thermal convective force on the 1DPC can assemble the colloidal particles that are dispersed in water solution, while photonic scattering force on the same 1DPC caused by propagating evanescent waves can guide these particles. Additionally, in the 1DPC, one internal mode can be excited that has been seldom noticed previously. This mode shows an ability to assemble particles over large areas even when the incident power is low. The assembly and the guidance of colloidal particles on 1DPC are switchable just through tuning the polarization and angle of the incident laser beam. Numerical simulations were carried out, which are consistent with these experimental observations.

KEYWORDS: One-dimensional photonic crystal, colloidal particles, thermal convection force, optical scattering force, evanescent waves, internal mode

The optical tweezer's broad appeal has come about because of its non-contact nature and microscopic object can be picked up, delivered to a desired place in order to facilitate the act of a measurement or reaction, and then brought back to an initial position [1,2]. However, due to the limited magnitude of optical trapping forces at high input power (usually up to 10^2-10^3 mW) [3-5], it is difficult to assemble or guide large numbers of small objects that are dispersed in liquids [6,7]. Within this limit, it was found that evanescent waves of the dielectric or metal interface could manipulate particles over large areas at lower power. A colloidal particle placed in the vicinity of an evanescent wave will be guided along the direction of the evanescent wave vector, by transferring the momentum of the propagating evanescent waves to a dielectric particle (photonic scattering force) [8-16]. Besides optical field, photothermal manipulation techniques provide versatile control of diverse species for colloidal particles, the strong temperature gradients of optothermal can cause optothermo-matter coupling phenomena through a combination of Marangoni convection, thermophoresis, thermoelectricity and photophoresis [17-20]. Many methods for large scale trapping of dielectric particles have been proposed by combining optical forces and optically induced thermal forces. Different competing forces dominate, leading to markedly different particle dynamics [21-24].

In this work, manipulations of colloidal particles that were placed on a dielectric multilayer photonic band gap (PBG) structure were investigated experimentally and numerically. This structure is called one-dimensional photonic crystal (1DPC) and has emerged as unique structure for exciting Bloch surface waves (BSWs) [25] that can be used in imaging, sensing, two-dimensional optical elements, and other applications [26-32]. In fact, except for the BSWs, evanescent waves can also be excited on the surface of this 1DPC through the total internal reflection (TIR). Due to the existence

of PBG, these evanescence waves are sensitive to the polarization and angle of the incident laser beam, and thus will induce different forces on the colloidal particles, which has not been fully explored before [33,34]. Furthermore, for this 1DPC, one internal mode can be excited inside the multilayers and then electromagnetic field will be localized inside the 1DPC. Under continuous illumination of laser beam, heat will certainly be generated inside the 1DPC and then diffuse to the surface. The effect of this heat on manipulation of colloidal particles has also not been carefully investigated before [35]. In this work, manipulation of colloidal particles enabled by the evanescent waves and the internal mode of the 1DPC were investigated experimentally and numerically, which showed different phenomena from the manipulations of colloidal particles by using evanescent waves on a conventional glass/water interface [36].

RESULTS AND DISCUSSION

Configurations of the experimental set-up and the 1DPC

Figure 1A shows a schematic diagram of the experimental set-up, which was based on an inverted optical microscope. The center wavelength of the laser beam is 640nm, which is used for the optical manipulations. The polarization of the incident laser beam was controlled using a polarizer and a half-wave plate. Using a pair of scanning galvanometers and a focusing lens, the expanded and collimated incident laser beam could then be focused on any point in the back focal plane (BFP) of the objective (100×, numerical aperture (NA) of 1.49) [32]. The expanded and collimated beam would then exit the objective and strike the substrate at a specific angle of incidence (θ). This angle (θ) is determined by the position of the focused point on the BFP, as illustrated in Fig. 1A. The propagation direction of the incident beam relative to the normal plane of

the multilayer structure can be defined using the two angles (θ and Ψ) illustrated in Fig. 1A. Use of the high-speed scanning galvanometers means that the angles of incidence (θ and Ψ) can be changed very quickly (in less than 1 ms). The laser beam reflected from the 1DPC was rejected by a band-pass filter, meaning that only the light from the white-light illuminator could reach the camera, then the motions of the manipulated particles could be monitored clearly.

The dielectric multilayers were fabricated via plasma-enhanced chemical vapor deposition (PECVD; PlasmaPro System 100, Oxford) of SiO_2 and Si_3N_4 on a standard microscope cover glass (12-548C, Fisher Scientific, 0.17mm thickness) under a vacuum of <0.0133 pa and at a temperature of 300°C. The thicknesses of these layers are 66 nm (Si_3N_4) and 110 nm (SiO_2), respectively. There are fourteen layers in total. The thickness of the top SiO_2 layer was approximately 200 nm, as shown in Fig. 1B. The plane of incidence is X-Z plane (Fig. 1B). One drop of a water-based solution containing the colloidal particles was placed on the 1DPC. The mean diameter of these particles is approximately 2 μm. To check the response of the 1DPC to incident beams with different polarizations, an expanded white light beam was used to fully fill the rear aperture of the objective and was then focused onto the 1DPC. The reflected light was collected using the same objective (100×, NA of 1.49). The BFP of the objective was imaged using a scientific complementary metal-oxide-semiconductor (sCMOS) camera. A band-pass filter with a center wavelength of 640 nm was placed in front of the sCMOS camera to filter the reflected light. The captured BFP image of the light reflected from the 1DPC is shown in Fig. 1C. The white line with the double arrowhead on Fig. 1C represents the incident polarization. The objective lens is axially symmetrical with respect to the optical path, so, as illustrated in the BFP image, the incident light along the direction Ψ = 0° has transverse-electric (TE) polarization, while that along the direction Ψ = 90° has transverse-magnetic

(TM) polarization, relative to the surface plane of the 1DPC. Based on the known NA of the objective, the TIR angle for the TM incident beam can be derived to be θ = 62°, which is consistent with the results of the numerical calculation (arc sin (1.33/1.515)). This BFP image clearly shows that the intensity of the reflected light from the TE-polarized incident beam differs from that of the TM-polarized incident beam, which indicates that the response of the 1DPC to the incident beam is polarization-dependent. There is also a pair of dark arcs showing on the BFP image, which is the signature of excitation of an internal mode. The excitation angle can be derived to be about θ = 65°. Based on the known incident polarization, it can be deduced that this internal mode can only be excited using a TE-polarized beam [35]. The difference was illustrated more clearly in the incident angle-dependent reflectance curves shown in Fig. 1D, which was calculated based on the transfer matrix method (TMM) [37]. According to the TMM, the field expansion coefficients in the glass substrate and water can be related via the matrix product

$$\begin{pmatrix} A_{water} \\ B_{water} \end{pmatrix} = \begin{pmatrix} m_{11} & m_{12} \\ m_{21} & m_{22} \end{pmatrix} \begin{pmatrix} A_{glass} \\ B_{glass} \end{pmatrix} \quad (1)$$

where A_{glass} and B_{glass} are the amplitudes of the incident and reflected waves in the glass substrate, respectively. A_{water} and B_{water} are the amplitudes of the incident and reflected waves in the water, respectively. m_{ij} (i,j = 1, 2) is the matrix element of transfer matrix. In this work, the incident beam is incident on the dielectric multilayer from the glass substrate (A_{glass} = 1, B_{water}= 0). Then, the reflectance of the incident beam can be expressed as

$$R = \left| \frac{B_{glass}}{A_{glass}} \right|^2 = \left| -\frac{m_{21}}{m_{22}} \right|^2 \quad (2)$$

When the incident beam is TM-polarized, there is a broad dip (indicating low reflectivity) below the TIR angle (62°), which is consistent with the BFP image. In contrast, when the incident

beam is TE-polarized, no such broad dip appears below the TIR angle, but a narrow dip appears at 66.9° that corresponds with the internal mode excitation resonance. This calculated angle is nearly consistent with that measured using the BFP imaging technique (65°, Fig. 1C).

Experimental demonstrations on assembly and guidance of colloidal particles placed on 1DPC

At first, the angle of incidence of the laser beam was set at about 63°, which is larger than the TIR angle, but lower than the angle for exciting the internal mode. The power of the incident laser beam was measured when a sensor of power meter (Microscope power sensor, S170C, Thorlab) was placed on the front focal plane of the objective (replacing the sample, as shown in Fig. 1A) and was measured to be approximately 16 mW. The power measured is that of the laser beam emitting from the objective. This power can be seen as the power of the light that reach the substrate of the dielectric multilayer (glass, Fig. 1B). It can be seen as the incident power. This incident power does not change when we change the incident angle or incident polarization.

The illumination region of the laser beam is illustrated with the red-dashed circles drawn in Fig. 2A-2D. When the incident beam was TE-polarized, we find a large-scale migration of colloidal particles radially towards the center of the illumination region and aggregated into hexagonal close-packed colloidal crystals. The number of particles on Fig. 2A is much less than that on Fig. 2D, meaning that particles with locations beyond the illumination region or even field of view (FoV) of the objective were also dragged into the illumination region. Once the incident polarization was changed to be TM, the particles continue to migrate toward the illumination region at first, but after they enter into the illumination region, these colloidal particles were rapidly guided along the propagation direction of the excited evanescent waves and stop around the edge of the illumination

region as shown in Fig. 2E to 2H. More clearly demonstrations on the assembly and guidance of the colloidal particles using the two types of polarizations can be found in Video-1 [38]. These phenomena demonstrate directly that in a 1DPC containing a PBG, the evanescent waves produced by the TE-polarized beam have a totally different effect on the colloidal particles to that produced by the TM-polarized beam, which has not previously been observed in the case of evanescent waves on a water/glass interface [36].

To qualitatively demonstrate the guidance of the particles (It only happened inside the laser illumination region, meaning the movement of the particles along the propagating direction of the laser beam on the X-Y plane (the direction is shown with the arrowhead on Fig. 3A and 3E)), we prepared dilute samples and measure the guiding velocity of individual colloid particle inside the laser illumination region. As shown in Fig. 3A-3H, the incident angle was set as about 62^{o} where both the TM- and TE-polarized laser beam can guide the particles in the laser illumination region, but with different average velocity (5.37 μm/s for TM-polarized and 2.23 μm/s for TE-polarized beam). The guiding velocity at other incident angle was also measured as shown in Fig. 3I. For each incident angle, the velocities of 3 individual particles were measured and then averaged to get the final velocity at this angle. The experimental results clearly demonstrate the guiding velocity in the case of TM-polarized beam is larger than that of TE-polarized beam. For the two polarized beams, when the incident angle was increased, the guiding velocity will reach zero (the particle will be stable on the image), meaning that the individual particle will not be guided along the propagating direction of the laser beam.

When the incident angle was still increased (such as to 65^{o}), we will find the assembly of the particles outside and inside the laser illumination region for both TM- and TE-polarized laser beam.

According to the BFP image (Fig. 1C) and reflection curve (Fig. 1D), the internal mode in the 1DPC appears only at the TE-polarized beam with the incident angle at about 65°. To test the changes in manipulations of the colloidal particles, corresponding experiments at this incident angle were carried out. The incident power was approximately 4 mW. Fig.4A–4D show that the colloidal particles were assembled quickly, even when the incident power was only one quarter of that used in the experiments in Fig. 2A–2D. In contrast, at the same laser power (4 mW) and the same incident angle, particles assembled very slowly under TM polarization (Fig. 4E–4H). Similarly, as Fig. 2A-2D, the number of particles on Fig. 4A (or Fig. 4E) is also much less than that of Fig. 4D (or Fig.4H), so the particles beyond the FoV of the microscope are also attracted to the laser illumination region.

As shown in the Video-1 [38], Fig. 2 and Fig. 4, the particles outside of the laser illumination region were attracted or assembled to the center, under both the TM- and TE-polarized illumination and different incident angle. This average assembly-velocity also can be measured from the two images, such as those shown in Fig. 5A and Fig.5B that were recorded at t = 0s and t = 60s, respectively. Here, the assembly velocities of three individual particles (P3, P4, and P5) were calculated and then an average velocity was obtained as shown in Fig. 5C. It should be noted that this assembly velocity means the drag speed of the particles from outside of the laser illumination region (Fig. 5A) to the boundary of the illumination region (Fig. 5B). The assembly velocity under different incident angles (63^{o} and 65^{o}), incident power (4 mW, and 16 mW), and polarization (TE and TM) were all measured as summarized in Fig. 5C. It is clearly show that the drag speed is the largest when the internal mode was excited (TE-polarized, P =16 mW, and incident angle is 65^{o}).

Numerical simulations on the photonic force and thermal convection.

To derive the mechanisms for particles assembly and guidance as shown in Figs. 2, 3,4 and 5 numerical simulations were performed as following. In our experiments, the angle of incidence was larger than the critical angle and the evanescent waves were generated on the surface of 1DPC. These evanescent waves will induce scattering forces on the colloidal particles that is along the propagating direction of the waves, and gradient force that is pointed to the multilayer. Three-dimensional Finite-Difference Time-Domain (FDTD) simulations [39,40] were performed to calculate the angular-dependent scattering optical force (F_{Sx}) and photonic gradient force (F_{Gz}) as shown in Fig. 6A and 6B. In the simulations, the dielectric multilayers consisted of alternating layers of SiO_2 (low refractive index, $n = 1.474 + i*10^{-4}$) and Si_3N_4 (high refractive index, $n = 2.498 + i*10^{-3}$) at a wavelength of 640 nm. The refractive indices of the water and the glass substrate were 1.33 and 1.515, respectively. The refractive index of the colloidal particle is 1.59. The incident power is set at 16 mW.

Fig.6A clearly demonstrates that the photonic scattering forces by TM-polarized beam is stronger than that by TE-polarized beam. The scattering forces decreases with increasing incident angle (from 62° to 67°, larger than the critical angle). Fig. 6B also demonstrate that the photonic gradient force will drag the particle to the dielectric multilayer (the force is negative) when the incident angle is larger than the TIR angle (62^{o}) [36]. It also demonstrated that the photonic gradient force by the TM-polarized beam is larger than that by the TE-polarized beam. These numerical results can be explained through the electric-field distributions of the evanescent waves in Fig. 6C – 6F. The intensity of the evanescent waves on the 1DPC/water interface in the case of TM-polarized incident beam (Fig. 6D, Fig. 6F) is stronger than that of TE-polarized incident beam (Fig. 6C, Fig. 6E),

when the incident angle of the two polarized beams was the same. The stronger the electromagnetic field at the water/1DPC interface, the larger the scattering force enabled by this optical field. Similarly, for the TM-polarized incident beam, with the increasing incident angle, the intensity of the evanescent waves on the 1DPC/water interface decreases, and then the scattering force will weaken, such as that on Fig. 6D comparing with that on Fig. 6F.

The scattering force enabled by the evanescent waves can be used to explain the guidance of colloidal particles inside the laser illumination region as shown in Fig. 2E-2H and Fig. 3, where the strong scattering force by TM-polarized beam can guide the motion of the particles along the propagating directions of the evanescent waves. This guidance did not happen when the polarization was switched to TE (Fig. 2A-2D), or the incident angle was increased (Fig. 4), where the scattering forces enabled by the propagating evanescent waves was highly decreased to nearly zero as shown in Fig. 6A. Another evidence that the guidance is due to the optical scattering force, is that this guidance will stop when the particles were outside of the laser illumination region (as clearly shown in Video-1 [38]) where there is no electric field.

On the contrary, for the assembly of the particles, as demonstrated in the experimental section (Fig. 2A-2D, Fig. 4 and Fig. 5, Video-1 [38]), even particles beyond the laser illumination region where there are no electromagnetic fields, can be assembled. So, the assembly of particles is due to a long-range interaction and cannot be attributed to the optical scattering or gradient force. When we return to the electric field distributions on Fig. 6C, 6E and 6F, we find that the electric-field inside the multilayer is stronger than that on the 1DPC/water interface. Due to the intrinsic loss of the dielectric multilayers, heat will unavoidable be generated under continuous illumination of laser beam (Fig.1B) and will result in the temperature gradient on the 1DPC. We

deduce that the mechanism for the assembly of particles is due to the temperature gradient induced convective flows of the water solution, which is consistent with the phenomena of long-range capture of microparticles around the beam center by the generation of the local heat [24, 41].

In order to verify this judgement, COMSOL Multiphysics Ver. 5.4 [42] was used to conduct the thermal convective flow analysis with the same optical configuration as shown Fig. 1B. For simplification, the velocity of the water flow is stimulated based on a two-dimensional (2D) heat conduction, the thicknesses of the water film were set at 100 μm and the initial temperature of the system was set to 293.15 K. All other structural parameters are the same as that shown in Fig.1B.

Fig. 7 show the simulation results, where the arrow indicates the flow direction of water and can also represent the direction of the convective force enabled on the particles. From the flow directions (Fig. 7A - 7D), we can judge that the colloidal particles will be attracted to the center of the illumination region (X =0 μm), which is attributed to the temperature gradient induced convective flows of the water solution. The scale-bars (right-hand of each image) on Fig. 7 represents the flow velocity, which can also represent the magnitude of the convective forces enabled on the colloidal particles.

When comparing Fig. 7A and 7B (corresponding to experimental results shown in Fig.2, the incident angle was 63^{o}), the convective forces induced by the temperature gradient under illumination of TE- and TM-polarized laser beam are nearly the same, hence colloidal particles would be assembled in these two cases, which are consistent with the experimental results shown in Fig.5, where the colloidal particles outside of the laser illumination region can be assembled and attract to the laser illumination region at nearly the same assembly velocity (incident angle was 63^{o}

and incident power is 16 mW, for both TM and TE-polarized illumination). When these particles were attracted into the laser illumination region, as shown in Fig. 2, the TM-polarized illumination will guide the particles along the propagating direction of the laser beam in the X-Y plane (Fig. 2E-2H, Video-1 [38]), however, the TE-polarized beam will further attract the particles to the center and increase the assembly (Fig. 2A-2D, and Video-1 [38]). This difference inside the laser illumination region can be explained from the calculated optical scattering force as shown in Fig. 6A. When the incident angle was 63^{o}, the optical scattering force is much stronger for TM-polarized illumination, which will suppress the convective force, and then induce the guidance of the particles along the propagating directions of the evanescent waves (Fig. 2E-2H and Fig. 3). On the contrary, in the case of TE-polarized illumination, the scattering force is near zero, then the convective force will be dominant, and result in the assembly as shown in Fig. 2A-2D.

When the incident angle was increased, such as to 67^{o}, due to the more confinement of the electric field inside the 1DPC (especially for the internal mode excited by TE-polarized beam, Fig. 6E), more heat will be generated and then result in larger convective force (as shown in the scale bar on Fig. 7C). The incident power is only 4 mW, the flow velocity on Fig. 7C is still larger than that on Fig. 7A (the power is 16 mW). At this incident angle, the optical scattering force for both polarizations is nearly zero (Fig. 6A), so the convective forces will be dominant, which results in the assembly of the colloidal particles as shown in Fig. 4A-4D.

When comparing Figs. 7C and 7D, we can find the flow velocity in the case of TM-polarized illumination is much smaller than that of TE-polarized illumination, which can be attributed to the electric field distribution inside the 1DPC (Fig.6E and Fig. 6F). The smaller flow velocity will result in smaller convective force, and the assembly speed of colloidal particles will be much smaller, which

are consistent with the experimental results shown in Fig. 4E-4H and Fig.5C (the assembly velocity in the case of TM-polarized beam (0.122 μm/s) is much smaller than that of TE-polarized beam (0.738 μm/s) with incident angle at 65^{o}, the power was 4 mW).

From the simulated flow directions as shown in Fig. 7, we notice that the assembly particle (around the position X =0 μm) can be pushed upward and away from the water/1DPC interface, if the convective force is larger than the gravity of the particle. This was verified by our experimental results as shown in Fig. 8. The TE-polarized beam was used to excite the internal mode of the 1DPC. When the incident power was increased, more heat would be generated inside the multilayer structure, resulting in the stronger convective force. When the incident power was only 5 mW, the colloidal particles were organized into closely-packed hexagonal colloidal crystals (see Fig. 8A and 8B). As the incident power increased, reaching up to 12 mW, the number of organized particles in the illuminated region (marked using a dashed circle) decreased under continuous illumination, as shown in Fig. 8C and 8D. A clearer demonstration of the escape of these organized particles from the illuminated region is presented in Video-2 [43], showing that the particles was pushed upward due to the larger convective force than the gravity of the particle.

CONCLUSIONS

In summary, we have demonstrated for the first time that evanescent waves on an all-dielectric 1DPC allow the use of combined optical and thermal forces in either guiding or assembling colloidal particles, simply by tuning the polarization and angle of the incident laser beam. It creates an optical conveyor belt for the sampling and sorting of large-scale assemblies of micro-objects, which indicates a new potential use for the 1DPC. These phenomena have not been

observed for evanescent waves excited on a conventional water/glass interface. The mechanism of this guidance and assembly was analyzed from the competition between the optical scattering force and optical induced thermal convective force. When the optical scattering force is larger, the particles will be guided along the direction of the propagating evanescent waves inside the laser illumination region, such as TM-polarized incidence and the incident angle was 63^{o}. On the contrary, when the convective force is larger, such as TE-polarized laser beams with incident angler larger than the TIR angle, the colloidal particles will be assembled from outside of the laser illumination region to the inside. If the convective force was increase further by using the high laser power, the assembly particles can be pushed away from the 1DPC substrate, because that the convective force becomes larger than the gravity of the particle.

It should be noted here that while our experiments were performed with a high-NA objective, they can also be achieved when using a high-refractive-index prism-based setup, where more colloidal particles can be accumulated at the excitation region; in addition, the motion areas for these particles will be larger because the excitation region on the prism is larger than that on the objective lens [41, 44]. However, the advantage of the objective-based experimental setup is also obvious; its imaging ability can be used to monitor the manipulation of the particles directly while also capturing surface-enhanced Raman spectra, and it can also be used to study light-induced self-assembly and optical binding interactions, along with the nonlinear properties of densely packed metal or dielectric particle arrays. To the best of our knowledge, we have described an optical microscope system that is capable of both guiding and trapping dielectric particles using only one laser beam for the first time. This method can be used for applications including accumulation, microfiltration and transportation of micro/submicroscale particles or biological materials.

Attracting of many particles in the illumination region when thermal convection is formed might find applications in research of prebiotic evolution. A main requirement in prebiotic studies of self-replicating systems and prebiotic metabolisms [24] are high concentrations of reaction partners. It appears likely that thermal convection force can cause reaction partners (similar as the colloidal particles used in our experiment) to be drawn to the center of the excited region, and then their concentrations can be highly increased. The ability to generate local heat inside the 1DPC substrate can also be used to develop thermophoretic tweezers that can be used to manipulate colloidal particles, living cells, and other bodies [45-47].

REFERENCES

[1] A. Ashkin, Optical trapping and manipulation of neutral particles using lasers, Proc. Natl. Acad. Sci. U. S. A. **94**, 4853-4860 (1997).

[2] A. N. Grigorenko, N. W. Roberts, M. R. Dickinson, and Y. Zhang, Nanometric optical tweezers based on nanostructured substrates, Nat. Photonics **2**, 365-370 (2008).

[3] K. C. Neuman, and S. M. Block, Optical trapping, Rev. Sci. Instrum **75**, 2787-2809 (2004).

[4] P. M. Hansen, V. K. Bhatia, N. Harrit, and L. Oddershede, Expanding the optical trapping range of gold nanoparticles, Nano Lett. **5**, 1937-1942 (2005).

[5] A. Lehmuskero, P. Johansson, H. Rubinsztein-Dunlop, L. M. Tong, and M. Kall, Laser Trapping of Colloidal Metal Nanoparticles, Acs Nano **9**, 3453-3469 (2015).

[6] A. Ashkin, J. M. Dziedzic, and T. Yamane, Optical Trapping and Manipulation of Single Cells Using Infrared-Laser Beams, Nature **330**, 769-771 (1987).

[7] A. Ashkin, J. M. Dziedzic, J. E. Bjorkholm, and S. Chu, Observation of a Single-Beam Gradient Force Optical Trap for Dielectric Particles, Opt. Lett. **11**, 288-290 (1986).

[8] V. Garces-Chavez, K. Dholakia, and G. C. Spalding, Extended-area optically induced organization of microparticies on a surface, Appl. Phys. Lett. **86,** 031106(2005).

[9] J. R. Arias-Gonzalez, and M. Nieto-Vesperinas, Optical forces on small particles: attractive and

repulsive nature and plasmon-resonance conditions, J. Opt. Soc. Am. A **20**, 1201-1209 (2003).

[10] D. Erickson, X. Serey, Y. F. Chen, and S. Mandal, Nanomanipulation using near field photonics, Lab Chip **11**, 995-1009 (2011).

[11] M. L. Juan, M. Righini, and R. Quidant, Plasmon nano-optical tweezers, Nat. Photonics **5**, 349-356 (2011).

[12] K. Wada, K. Sasaki, and H. Masuhara, Optical measurement of interaction potentials between a single microparticle and an evanescent field, Appl. Phys. Lett. **76**, 2815-2817 (2000).

[13] G. Volpe, R. Quidant, G. Badenes, and D. Petrov, Surface plasmon radiation forces, Phys. Rev. Lett. **96,** 238101 (2006).

[14] B. S. Schmidt, A. H. J. Yang, D. Erickson, and M. Lipson, Optofluidic trapping and transport on solid core waveguides within a microfluidic device, Opt. Express **15**, 14322-14334 (2007).

[15] M. Righini, G. Volpe, C. Girard, D. Petrov, and R. Quidant, Surface plasmon optical tweezers: Tunable optical manipulation in the femtonewton range, Phys. Rev. Lett. **100,** 186804 (2008).

[16] K. Wang, E. Schonbrun, P. Steinvurzel, and K. B. Crozier, Scannable Plasmonic Trapping Using a Gold Stripe, Nano Lett. **10**, 3506-3511 (2010).

[17] S. Duhr, and D. Braun, Why molecules move along a temperature gradient, Proc. Natl. Acad. Sci. U. S. A. **103**, 19678-19682 (2006).

[18] H. R. Jiang, H. Wada, N. Yoshinaga, and M. Sano, Manipulation of Colloids by a Nonequilibrium Depletion Force in a Temperature Gradient, Phys. Rev. Lett. **102,** 208301 (2009).

[19] E. Flores-Flores, S. A. Torres-Hurtado, R. Paez, U. Ruiz, G. Beltran-Perez, S. L. Neale, J. C. Ramirez-San-Juan, and R. Ramos-Garcia, Trapping and manipulation of microparticles using laser-induced convection currents and photophoresis, Biomed. Opt. Express **6**, 4079-4087 (2015).

[20] R. Piazza, and A. Guarino, Soret effect in interacting micellar solutions, Phys. Rev. Lett. **88,** 208302 (2002).

[21] H. B. Xin, and B. J. Li, Targeted delivery and controllable release of nanoparticles using a defect-decorated optical nanofiber, Opt. Express **19**, 13285-13290 (2011).

[22] M. Righini, C. Girard, and R. Quidant, Light-induced manipulation with surface plasmons, J. Opt. A: Pure Appl. Opt. **10,** 093001 (2008).

[23] J. Chikazawa, T. Uwada, A. Furube, and S. Hashimoto, Flow-Induced Transport via Optical

Heating of a Single Gold Nanoparticle, J. Phys. Chem. C **123**, 4512-4522 (2019).

[24] D. Braun, and A. Libchaber, Trapping of DNA by thermophoretic depletion and convection, Phys. Rev. Lett. **89,** 188103 (2002).

[25] P. Yeh, A. Yariv, and C. S. Hong, Electromagnetic Propagation in Periodic Stratified Media .1. General Theory, J. Opt. Soc. Am. **67**, 423-438 (1977).

[26] Y. Augenstein, A. Vetter, B. V. Lahijani, H. P. Herzig, C. Rockstuhl, and M. S. Kim, Inverse photonic design of functional elements that focus Bloch surface waves, Light: Sci. Appl. **7**, 104 (2018).

[27] A. Angelini, A. Lamberti, S. Ricciardi, F. Frascella, P. Munzert, N. De Leo, and E. Descrovi, In-plane 2D focusing of surface waves by ultrathin refractive structures, Opt. Lett. **39**, 6391-6394 (2014).

[28] I. V. Soboleva, V. V. Moskalenko, and A. A. Fedyanin, Giant Goos-Hanchen Effect and Fano Resonance at Photonic Crystal Surfaces, Phys. Rev. Lett. **108** , 123901 (2012).

[29] D. A. Shilkin, E. V. Lyubin, I. V. Soboleva, and A. A. Fedyanin, Direct measurements of forces induced by Bloch surface waves in a one-dimensional photonic crystal, Opt. Lett. **40**, 4883-4886 (2015).

[30] F. Giorgis, E. Descrovi, C. Summonte, L. Dominici, and F. Michelotti, Experimental determination of the sensitivity of Bloch Surface Waves based sensors, Opt. Express **18**, 8087-8093 (2010).

[31] E. Descrovi, T. Sfez, M. Quaglio, D. Brunazzo, L. Dominici, F. Michelotti, H. P. Herzig, O. J. F. Martin, and F. Giorgis, Guided Bloch Surface Waves on Ultrathin Polymeric Ridges, Nano Lett. **10**, 2087-2091 (2010).

[32] Y. Kuai, J. X. Chen, X. Tang, Y. F. Xiang, F. Y. Lu, C. F. Kuang, L. Xu, W. D. Shen, J. J. Cheng, H. Q. Gui, G. Zou, P. Wang, H. Ming, J. G. Liu, X. Liu, J. R. Lakowicz, and D. G. Zhang, Label-free surface-sensitive photonic microscopy with high spatial resolution using azimuthal rotation illumination, Sci. Adv. **5,** eaav5335 (2019).

[33] J. D. Joannopoulos, Photonic Crystals Molding the Flow of Light, J. Occup. Med. Toxicol. **375**, 278-278 (1995).

[34] J. X. Chen, D. G. Zhang, P. Wang, H. Ming, and J. R. Lakowicz, Strong Polarization Transformation of Bloch Surface Waves, Phys. Rev. Appl. **9** , 024008 (2018).

[35] D. G. Zhang, R. Badugu, Y. K. Chen, S. S. Yu, P. J. Yao, P. Wang, H. Ming, and J. R. Lakowicz, Back focal plane imaging of directional emission from dye molecules coupled to one-dimensional photonic crystals, Nanotechnology **25,** 145202 (2014).

[36] S. Kawata, and T. Sugiura, Movement of Micrometer-Sized Particles in the Evanescent Field of a Laser-Beam, Opt. Lett. **17**, 772-774 (1992).

[37] E. Anemogiannis, E. N. Glytsis, and T. K. Gaylord, Determination of guided and leaky modes in lossless and lossy planar multilayer optical waveguides: reflection pole method and wavevector density method. J. Lightwave Technol.**17**,929 (1999).

[38] See Supplemental Material at [URL will be inserted by publisher] for [Assembly of the colloidal particles using the TE-polarized beam and guiding the particles using the TM-polarized beam when the angle of incidence was set at 63°. The red ring indicates the position of the laser illumination region].

[39] A. Taflove, and S. C. Hagness, Computational Electrodynamics: The Finite-Difference Time-Domain Method, 3rd edition, J. Comput. Methods Sci. Eng. (2005).

[40] P. H. Jones, O. M. Maragò, G. Volpe, Optical Tweezers: Principles and Applications, Cambridge University Press (2015)

[41] V. Garces-Chavez, R. Quidant, P. J. Reece, G. Badenes, L. Torner, and K. Dholakia, Extended organization of colloidal microparticles by surface plasmon polariton excitation, Phys. Rev. B **73** , 085417 (2006).

[42] http://www.comsol.com

[43] See Supplemental Material at [URL will be inserted by publisher] for [Escape of the organized particles from the illuminated region when the incident power increased. The internal mode was excited using the TE-polarized beam. The red ring indicates the position of the laser illumination region].

[44] M. Siler, T. Cizmar, A. Jonas, and P. Zemanek,Surface delivery of a single nanoparticle under moving evanescent standing-wave illumination, New J. Phys. **10**, 113010 (2008).

[45] L. Lin, M. S. Wang, X. L. Peng, E. N. Lissek, Z. M. Mao, L. Scarabelli, E. Adkins, S. Coskun, H. E. Unalan, B. A. Korgel, L. M. Liz-Marzan, E. L. Florin, and Y. B. Zheng, Opto-thermoelectric nanotweezers, Nat. Photonics **12**, 195-201 (2018)

[46] L. H. Lin, X. L. Peng, X. L. Wei, Z. M. Mao, C. Xie, and Y. B. Zheng, Thermophoretic Tweezers for Low-Power and Versatile Manipulation of Biological Cells, Acs Nano **11**, 3147-3154 (2017).

[47] L. H. Lin, E. H. Hill, X. L. Peng, and Y. B. Zheng, Optothermal Manipulations of Colloidal Particles and Living Cells, Acc. Chem. Res. **51**, 1465-1474 (2018).

ACKNOWLEDGMENTS

This work was supported by National Nature Science Foundation of China (61427818, 11774330), Ministry of Science and Technology of China (2016YFA0200601), Anhui Initiative in Quantum Information Technologies, the Science and Technological Fund of Anhui Province for Outstanding Youth (1608085J02), Anhui Provincial Science and Technology Major Projects (18030901005), the Fundamental Research Funds for the Central Universities (WK2340000084), the foundation of Key Laboratory of Environmental Optics and Technology of Chinese Academy of Sciences (Grant No.2005DP173065-2019-XX), the Longshan Academic Talent Research Supporting program of SWUST (grant no. 17LZX626). D.G.Z is also supported by USTC Tang Scholar. JRL acknowledged supported by grants from the National Institute of Health (R01 GM125976 and R21 GM129561). The work was partially carried out at the University of Science and Technology of China's Center for Micro and Nanoscale Research and Fabrication.

Figures Caption

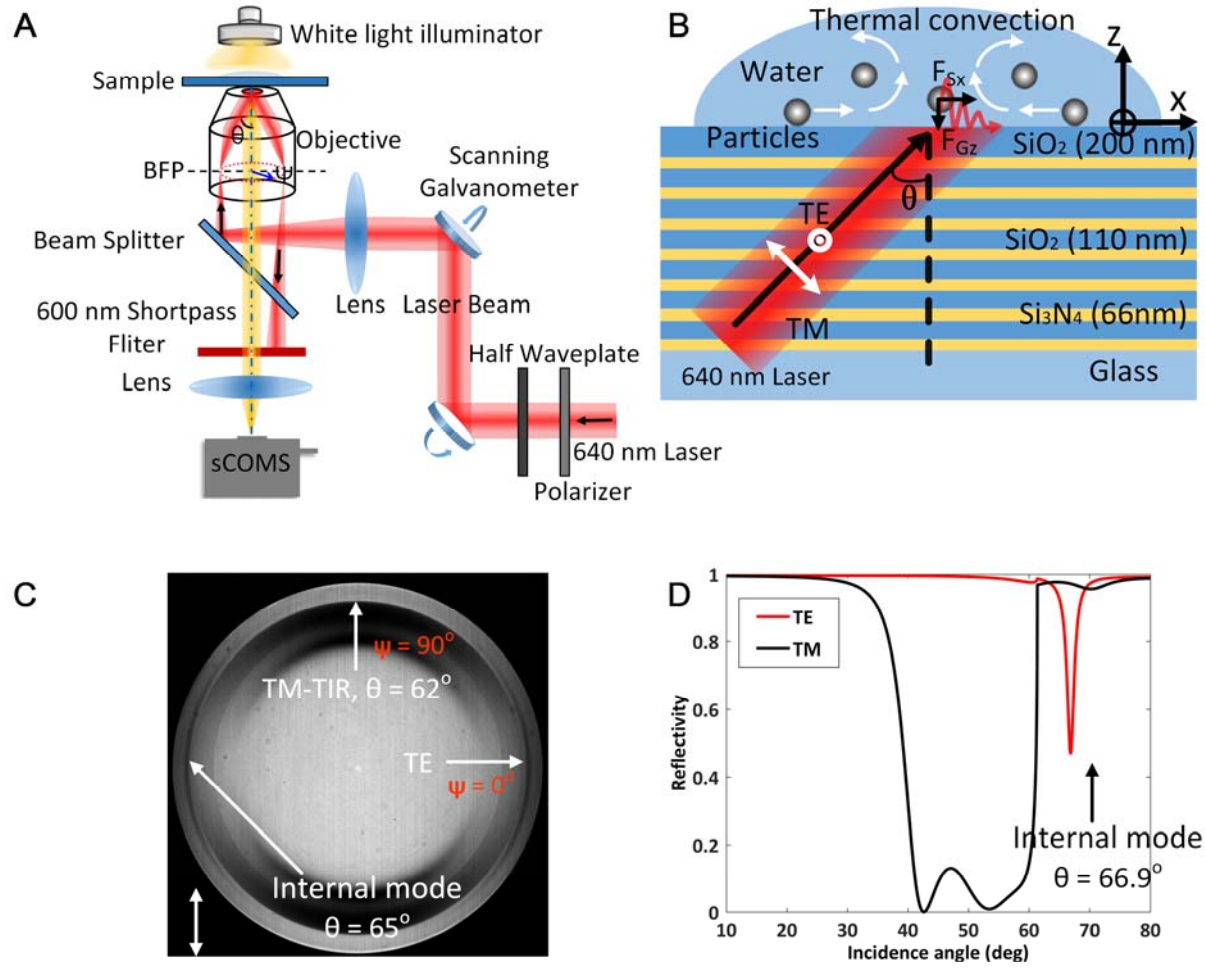

Figure 1: | Schematic of the experimental setup, the 1DPC and its BFP image, and the calculated angular-dependent reflection curves. (A) Experimental setup. BFP: back focal plane. (B) the sample on (A), the 1DPC acting as the substrate for the colloidal particles in a water-based solution. F_{Sx}, F_{Gz} are the photonic scattering force and photonic gradient force, respectively. (C) BFP image of the 1DPC. TIR: total internal reflection; TE: transverse-electric; TM: transverse-magnetic. The wavelength of the incident laser beam was 640 nm. (D) Calculated reflectance of the 1DPC versus angle of incidence under TE- and TM-polarized illumination.

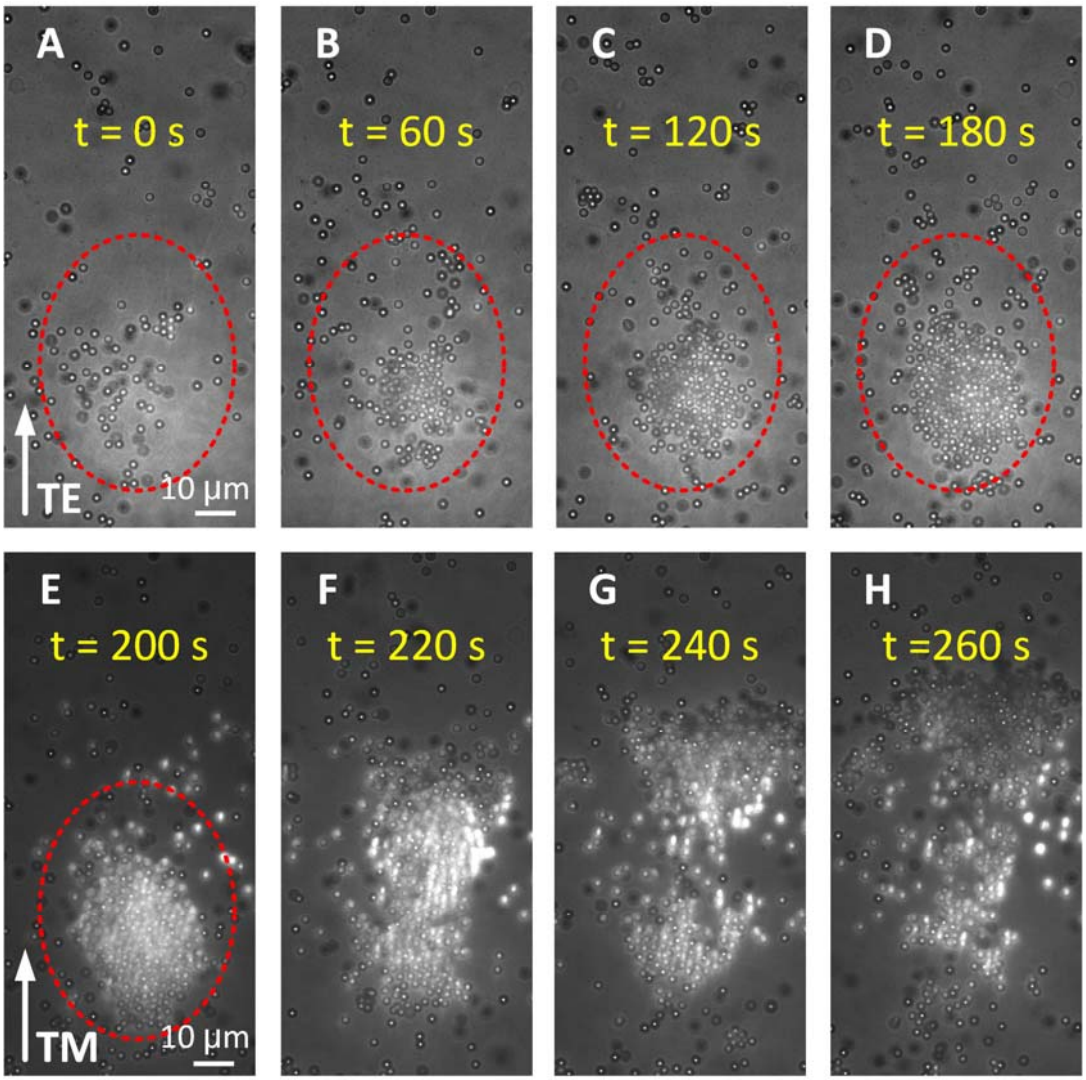

Figure 2: | Assembly and guidance of the colloidal particles with incident angle at about 63°. (A–D) The incident laser beam was TE-polarized. The colloidal particles were organized into hexagonal closely packed colloidal crystals during illumination. (E–H) The incident beam was changed to a TM-polarized beam; the packed colloidal particles were then guided along the propagation direction of the evanescent waves. The scale bar on (A) is also applicable to (B–H). The arrow lines on (A) and (E) show the propagation direction of the evanescent waves in each case. The incident laser beam power is approximately 16 mW. The dashed line circles indicate the illumination region of the laser beam.

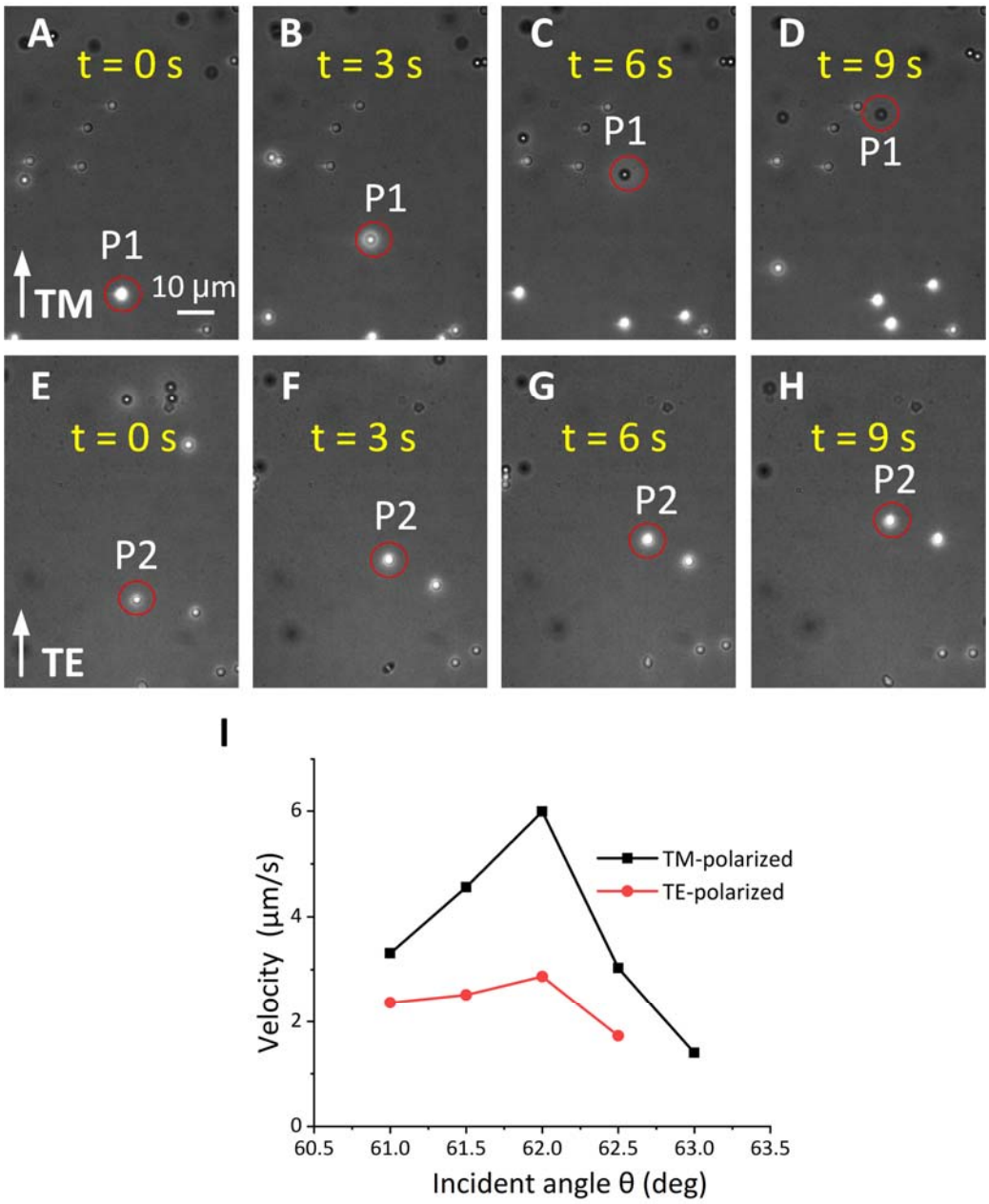

Figure 3: | Measuring the guidance velocity of the particle inside the laser illumination region. The incident power was 16 mW. (A–D) The incident beam was TM-polarized. (E–H) The incident beam was TE-polarized. the incident angle was 62^{o} (A-H). The position of the particle P1 and P2 on the image was changed with the time, which is due to the guidance. (I) the guiding velocity *vs.* incident angle for TM- and TE-polarized illumination. The scale bar shown on (A) is applicable to (B–H).

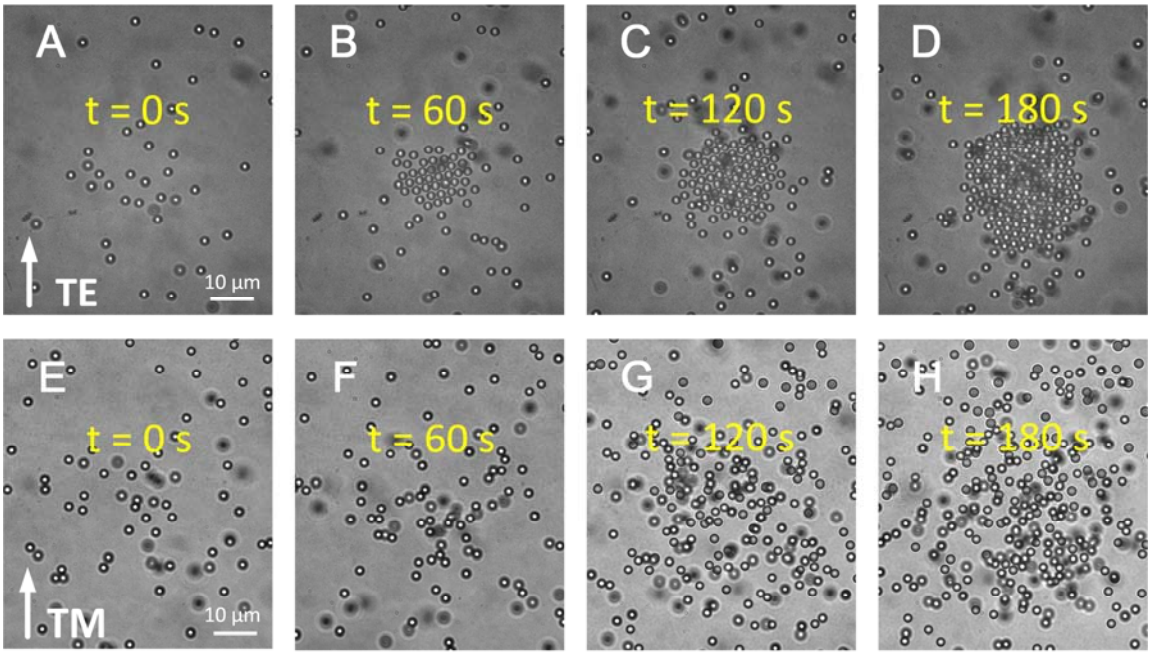

Figure 4: | Assembly of the colloidal particles with incident angle at approximately 65°. The incident power was 4 mW. (A–D) The incident beam was TE-polarized. (E–H) The incident beam was TM-polarized. The scale bar shown on (A) is applicable to (B–H).

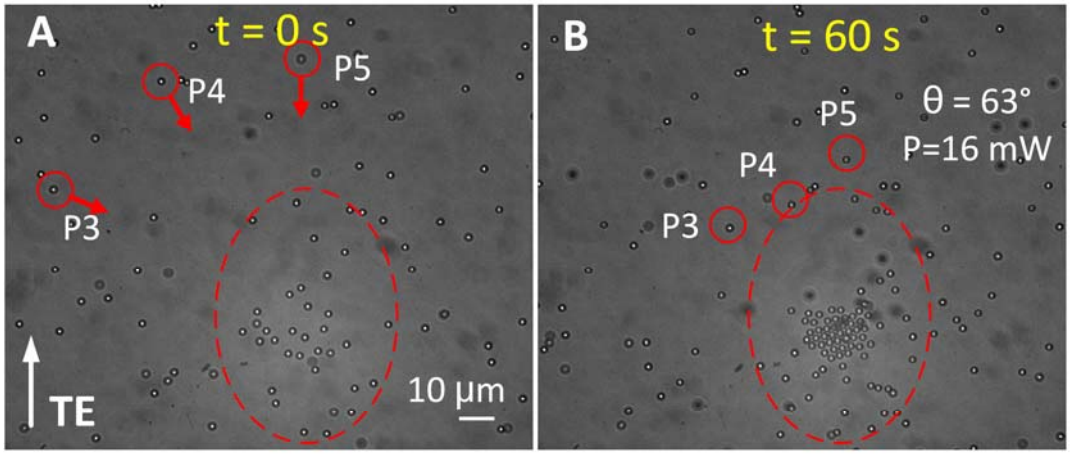

C

		TE-polarized	TM-polarized
63°	P=16 mW	0.607 μm/s	0.677 μm/s
65°	P=4 mW	0.738 μm/s	0.122 μm/s
	P=16 mW	5.508 μm/s	1.081 μm/s

Figure 5: | Measuring the assembly velocity of the particle outside of the laser illumination region. This assembly was due to the thermal convection force. (A)at the moment t = 0 s, three individual particles (P3, P4, and P5) were outside of and far away from the laser illumination region (marked with the red ring). (B) due to the laser illumination for 60 s, the three particle reach the boundary of the laser illumination region. The incident beam was TE-polarized, the incident power is 16 mW and the incident angle is 63^{o}. The scale bar shown on (A) is applicable to (B). (C) the averaged assembly velocity of the particle under various incident power, incident polarization, and incident angle.

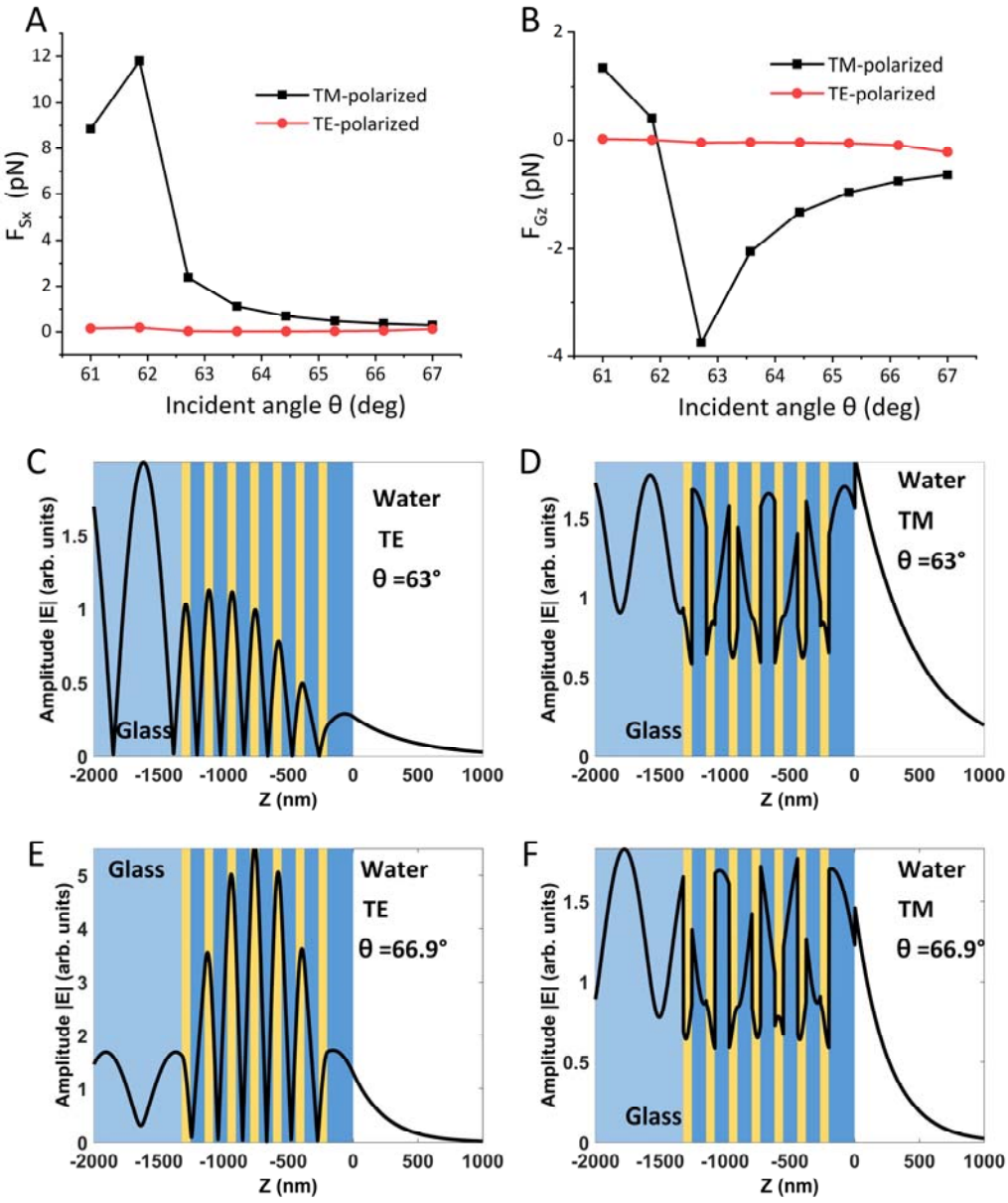

Figure 6: | Numerical simulations of the optical force and electric field distributions. (A) Calculated optical scattering force (F_{Sx}) and optical gradient force (F_{Gz}) as a function of the incident angle. (C, D) Electric field distributions under TE- (C) and TM-polarized (D) illumination, when the angle of incidence was fixed at 63°. (E, F) The same distributions when the angle of incidence was fixed at 66.9°, corresponding to the excitation angle for the internal mode, as shown in Fig 1(D). The position Z = 0 nm denotes the water/1DPC interface.

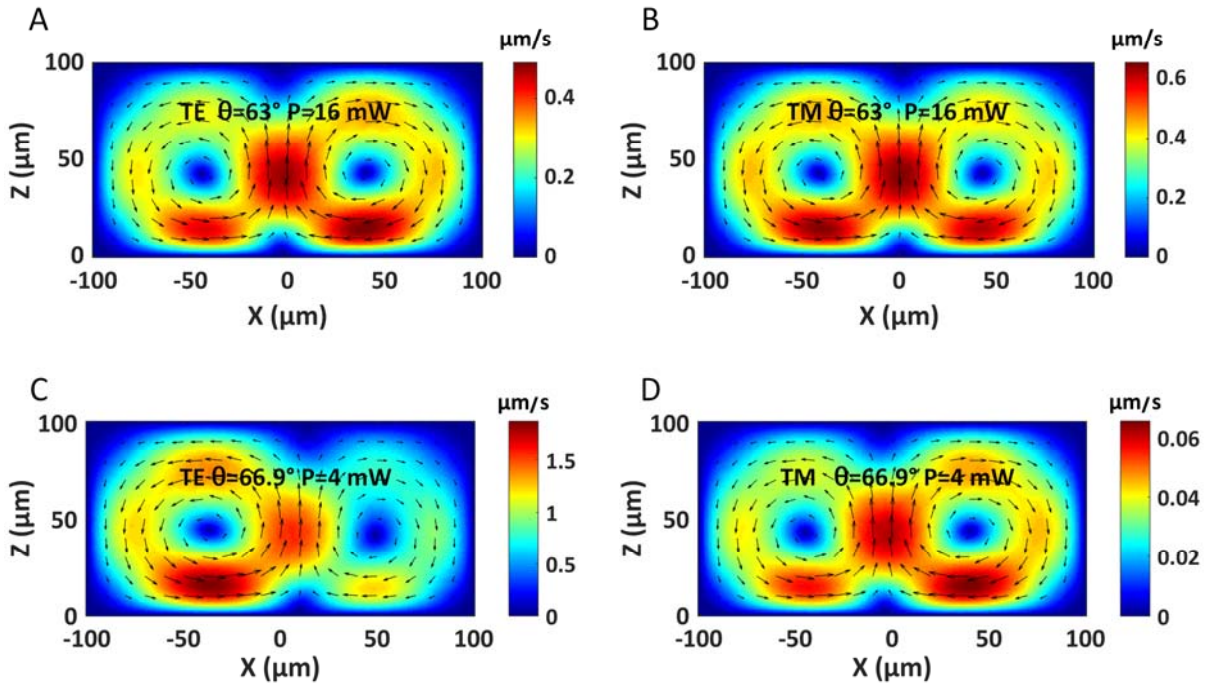

Figure 7: | Simulated 2D convective velocity maps around beam center (X= 0 μm). The arrows indicate the directions of water flow, and the scale-bar (left side of each image) express the magnitude of the velocity. (A-D) calculated fluid convection pattern under different polarizations (TE, TM), incidence angles (θ) and incident power (P). (A) TE-polarized, θ = 63°, P = 16 mW; (B) TM-polarized, θ=63°, P=16 mW; (C) TE-polarized, θ = 66.9°, P = 4 mW; (D) TM-polarized, θ = 66.9°, P = 4 mW.

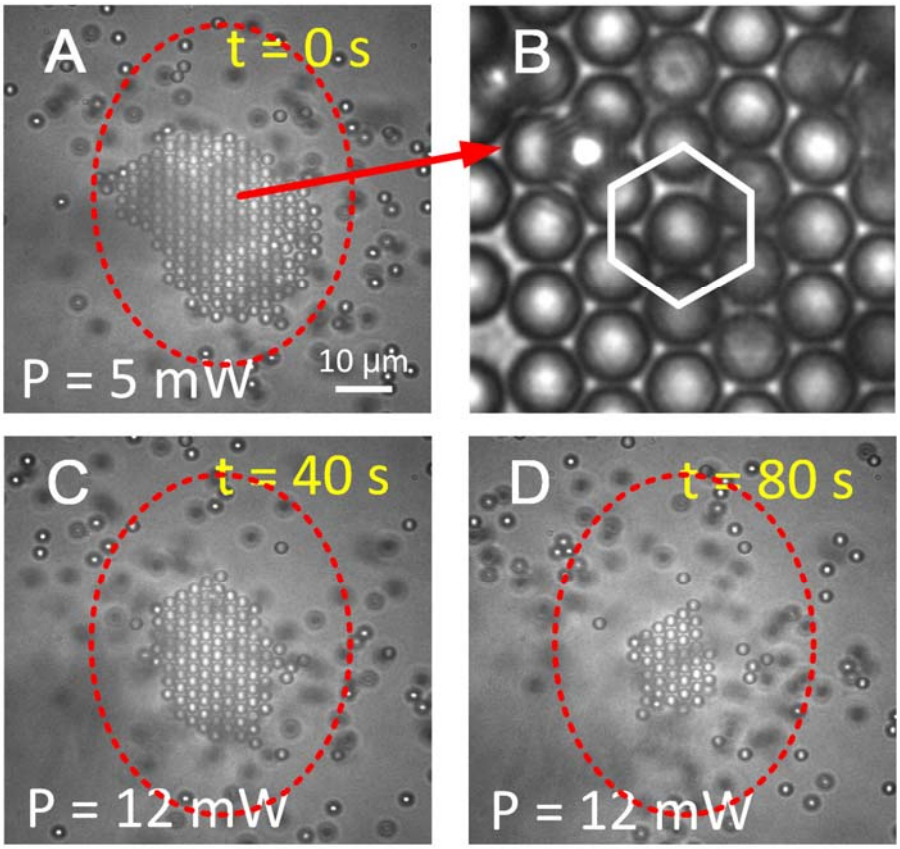

Figure 8: | Effect of incident power on assembly of the colloidal particles. The internal mode of the 1DPC was excited by TE-polarized laser beam. The incident power was increased from 5 mW (A) to 12 mW (C, D). (B) Enlarged graph of the assembled particles that shows the hexagonal pattern. The scale bar on (A) is also applicable to (C, D).